Stokes polarimetry imaging of rat tail tissue in a turbid medium: degree of linear polarization image maps using incident linearly polarized light

Paul J. Wu
Joseph T. Walsh Jr.
Northwestern University
Biomedical Engineering Department
Evanston, Illinois 60208
E-mail: jwalsh@northwestern.edu

Abstract. Illumination with incident linearly polarized light on tissue and polarization state measurements of the remitted light provide a means by which various tissue structures can be differentiated. A rat tail is embedded within a turbid gelatin such that there is a variable depth of medium above it. By varying the incident polarization angle (IPA) of the illuminating linearly polarized light, the geometry, and the orientation angle of the tissue, a series of 2-D degree of linear polarization image maps are created using our Stokes polarimetry imaging technique. The image maps show locations of the polarization-sensitive structures in the rat tail, including soft tissue, intervertebral disks, and tendons. The observed morphologies in the image maps indicate locations where the depolarization of light differs according to the tissue type and underlying layers. The data indicate the importance of varying the IPA, and that tissue dichroism and birefringence affect the degree of linear polarization image maps. Diagnostic information regarding subsurface tissue structures is obtained. [DOI: 10.1117/1.2162851]

Keywords: near infrared; tendon; birefringence; dichroism.

Paper 05023RR received Jan. 28, 2005; revised manuscript received Aug. 31, 2005; accepted for publication Sep. 1, 2005; published online Mar. 2, 2006.

1 Introduction

The use and detection of polarized light has shown promise for applications in biomedical diagnostic devices. The effect of biological tissue and turbid media on polarized light has been studied using transmission and reflectance methods from Stokes polarimetry and Mueller matrix polarimetry.[1–26] Since scattering events in a medium affect the polarization, direction, and phase of the propagating light, the use of polarized light allows differentiation among multiply scattered, weakly scattered, and ballistic photons.[1,2] Studies have shown the preservation of polarization over multiple scattering events.[2–4] Furthermore, differences in the scattering medium have been shown to influence the amount of depolarization.[5–9]

Various polarization imaging techniques in reflectance mode have been developed. For example, one can eliminate specular reflection and enhance the view of vasculature and pigmented lesions in skin using a cross-polarization technique.[10] Multiple wavelengths and cross-polarization, in conjunction with image differencing, allowed investigators to detect a deep, subsurface object in tissue.[11] Also, images formed using a polarization ratio, dependent on intensities from parallel and perpendicular analyzer positions, provide contrast that is useful in detecting differences in the superficial layers of various skin conditions.[12–14]

Polarimetry techniques,[15,16] most notably Mueller matrix polarimetry and Stokes polarimetry, have also been applied to the biomedical field. Mueller matrix polarimetry is used to measure the polarization-altering properties of a material/tissue, while Stokes polarimetry is used to measure the polarization state of light. Mueller matrix polarimetry relies on various arithmetic operations performed on intensity measurements formed with set incident polarizations (chosen among 0, 90, +45, −45 deg, RC, and LC) and with set analyzer types [chosen among 0, 90, +45, −45 deg, right circular (RC), and left circular (LC)] to determine the elements of the Mueller matrix.[17,18] In contrast, Stokes polarimetry only requires set combinations of analyzer types (chosen among 0, 90, +45, −45 deg, RC, and LC) but not predetermined incident polarizations to calculate the elements of the vector.[16] Therefore, in Stokes polarimetry, it is more convenient to vary the incident polarization angle compared to Muller matrix polarimetry.

The utility of using Mueller matrices has been shown in studies such as target detection in turbid media[19] and the differentiation of turbid media properties by average particle size and scattering coefficient.[20,21] Mueller matrix polarimetry can be extended to tissue imaging applications where measurements are made pixel by pixel over a region of interest. Thus far, Mueller matrix imaging polarimeters have been used primarily to investigate skin conditions.[22,23] Interpreting the individual elements in the Mueller matrix remains an active research area.

Most biomedical Stokes polarimetry studies have focused on using narrow coherent beams of light incident on a sample and measuring the degree of polarization of the light in trans-

Address all correspondence to Joseph Walsh, Biomedical Engineering, Northwestern University, 2145 Sheridan Road-L274, Evanston, IL 60208. Tel: (847)–491–3553; Fax: (847) 491–5341; E-mail: jwalsh@northwestern.edu

1083-3668/2006/11(1)/014031/10/$22.00 © 2006 SPIE

mission mode from the sample. Various techniques have been employed to measure the degree of polarization of laser-speckle fields,[24] the time-resolved Stokes vectors of various tissues,[25] and the degree of polarization of turbid media, tendon, myocardial, arterial, and adipose tissue.[26,27]

The long-term goal is the development of a technique that allows one to see alternations in the supporting tissue matrix. This matrix is most often formed by structures, e.g., collagen, that has significant form birefringence. Matrix alterations are known to occur in many disease states. In this work, we describe a near-infrared Stokes polarimetry imaging technique used to differentiate macroscopic tissue structures. The use of multiple IPAs provides an added dimension that can be used to aid in differentiating between normal and pathological regions. While variations or alterations in the tissue matrix may be difficult to see in an image map created with a single IPA, the use of many IPAs allows differentiation of tissue structures according to changes in the polarization state of remitted light. As an example, one disease where it is important to detect these tissue matrix differences is endometriosis. Here, conventional laparoscope-based optical imaging techniques have difficulty characterizing the deeper, subsurface endometrial lesions, and often a confirmation of tissue pathology awaits the postoperative analysis of the sample biopsy. The classical endometrial implant is a nodular lesion on the peritoneal wall, characterized by a variable degree of fibrosis and a wide range of pigmentations. Hence, the use of Stokes polarimetry imaging, while varying the incident polarization state, may provide utility in detecting changes in the tissue matrix collagen structure where lesions implant. While this technique could be applied eventually to aid in detection of pathological differences, such as those that occur at endometrial lesions, this initial study focused on a more elementary sample, namely rat tail tissue embedded within a turbid medium. Rat tail was chosen because of its simple yet varied structural composition. It consists of soft tissue, hard bony material, annulus fibrosis, and birefringent tendons all present naturally within various layers of the tail. Rat tails are also economical tissue parts and can be obtained conveniently in the university laboratory setting.

When using unpolarized light, the individual structures in the rat tail cannot be distinguished; only the general shape of the tail can be observed, as seen in Fig. 1. However, by using polarized light together with Stokes polarimetry, we investigated how the visibility of various known structures such as tendon, soft tissue, and intervertebral disks could be improved and contrasted between one another. In particular, the tendons present an excellent opportunity for us to image a birefringent material within a turbid medium. One of the parameters varied in this experiment is the incident polarization angle (IPA). Variations in IPA provide a way to probe tissue types that may have a differential response to a certain plane(s) of polarization. Furthermore, the use of a near-infrared wavelength provided a deep penetration depth such that the remitted signal included information from the subsurface tissue. By embedding the rat tail at varying depths in the turbid medium, the depth limitations for this imaging technique were explored. Different tissue geometries, in relation to the illumination and detection optics, were also investigated, as they can influence the features than can be resolved using this imaging technique.

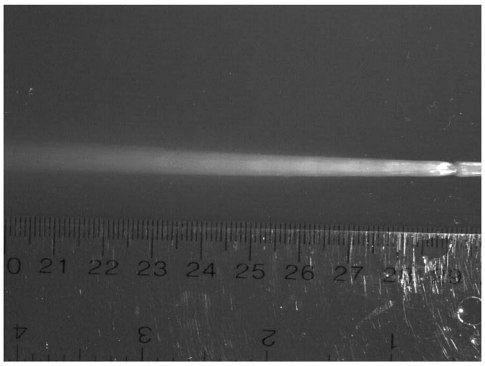

Fig. 1 Image of rat tail tissue taken while illuminated with unpolarized 940-nm light collected without the use of a polarimeter immediately before the camera. Note that only the basic shape of the rat tail can be seen; more detailed structures are not observed.

2 Materials and Methods

2.1 *Tissue Preparation*

Rat tails of euthanized adult Sprague-Dawley rats (350 to 400 g) were harvested immediately postmortem by transection at the proximal end. The tails were then frozen. Prior to the polarization imaging experiments, the rat tails were removed from the freezer and allowed to thaw at room temperature for 2 h. We have found that the freezing/thawing cycle did not affect the birefringence of the rat tail tendon significantly. The epidermal and dermal layers were dissected away, leaving the rat tail tendons, connective tissue, underlying tissue, and skeletal structure intact. Each ~12-cm-long rat tail was suspended inside a plastic container with the tail's long axis at a 15-deg angle with respect to the bench-top surface. A turbid-gel mixture [at 940 nm: $\mu_s' = 0.26\ \mathrm{cm}^{-1}$; $\mu_a = 0.025\ \mathrm{cm}^{-1}$; calculated by following the equations described in Farrel and Patterson[28]; transport mean free path $(\mathrm{mfp}') = 3.51$ cm] consisting of gelatin (Knox, Parsippany, New Jersey; 5.93-g powdered gelatin/100 ml of H_2O) and nondairy creamer (Jewel Food Stores, Boise, Idaho; corn syrup solids, partially hydrogenated soybean and/or canola oils, sodium caseinate, dipotassium phosphate, mono- and diglycerides, and silicon dioxide; 8.96×10^{-4} g/ml of H_2O) was used to fill the container and hence embed the tail. The container with the rat tail was refrigerated for 12 h to solidify the gelatin. The phantom optical properties were chosen to form an opaque medium such that the embedded rat tail could be placed at reasonable depths (i.e., on the order of several millimeters) below the gelatin surface, and yet when imaging the rat tail with unpolarized visible light, the appearance of the rat tail was masked. The rat tail was embedded diagonally so polarization signals could be measured from continuous rather than discrete depth levels. The tail geometry thus permitted the degree of linear polarization image maps of tissue to show information at depths up to ~20 mm below the gelatin surface in the image maps. Further, imaging the rat tail embedded at an angle allowed an investigation of the tilt-angle dependence of the birefringent tendons. While more than ten rat tails were used in developing the protocol and during data collection, the results shown here are all taken from one representative sample.

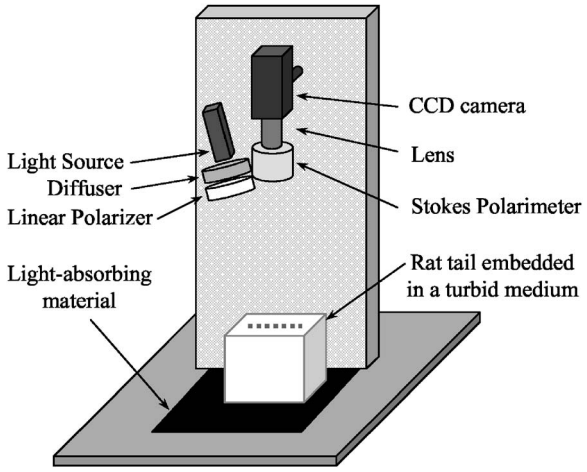

Fig. 2 Schematic diagram of the experimental setup. Randomly polarized 940-nm light from the diode-laser source passed first through a diffuser then a rotatable linear polarizer. The linearly polarized light struck the flat surface of the turbid gelatin at 15 deg. The rat tail was embedded in the gel at a tip angle of 15 deg from the horizontal. Remitted light traveling ±1 deg from vertical passed through the Stokes polarimeter and lens to the CCD camera.

2.2 *Polarization Imaging System*

Diffuse polarized light illuminated the rat tail embedded in the gelatin, and the remitted light was analyzed for its states of polarization. The experimental setup is shown in Fig. 2. The plastic container with the rat tail embedded in gelatin was placed on top of light-absorbing material. The light source was a fiber-coupled laser (Opto Power Corporation, Tucson, Arizona; model H01-D060-940-FCMS) emitting 940-nm radiation that was directed through a holographic diffuser (Physical Optics Corporation, Torrance, California; LSDKITCW60-50) and a linear polarizer (Corning, Corning, New York; Polarcor 900H-B2). The diffuser was used to scramble any preferred polarizations that may have been emitted by the largely unpolarized light source. The light was incident on the gel surface at an angle of 15 deg from vertical, which is as close to the normal that the physical limitations in the experimental setup would permit. The 940-nm radiation was chosen because of its relatively deep penetration depth into tissue. At the 15-deg angle of incidence, both the reflectivity of light from the gel surface and the transmission of light into the gelatin did not change significantly for all incident polarization angles. To vary the incident polarization angle (IPA), the linear polarizer was rotated. The intensity of light incident on the gel surface was constant for all IPAs.

The detection optics were set up such that the remitted light traveling within a range of ±1 deg with respect to the vertical axis was collected. The remitted light first passed through a Stokes polarimeter composed of a linear polarizer (Corning, Corning, New York; Polarcor 900H-B2) and a quarter-wave plate (Meadowlark Optics, Frederick, Colorado. AQM-100-840), each rotated accordingly to obtain the complete Stokes vectors. A camera lens (Canon, Japan; 100-mm f/16) focused the light onto a visible-NIR sensitive charge-coupled device (CCD) (Hitachi, Japan; KP-F120CL,10-bit resolution, 1392×1040 pixels). The detection optics (the lens and CCD system) were determined to be polarization insensitive: during calibration tests, the quantified standard deviation of the intensity over all linear polarization angles and elliptical polarizations was never more than three levels out of a dynamic range of 1024 levels. Images were transferred to a PC (Dell, Round Rock, Texas; Precision Workstation 530) via an image acquisition card (National Instruments, Austin, Texas; PCI-1428). Image processing and analysis were carried out using IDL v5.6 (Research Systems Incorporated, Boulder, Colorado) and Vision Builder v6.1 (National Instruments, Austin, Texas).

2.3 *Image Processing and Algorithms*

The Stokes vector $[\mathbf{I}\ \mathbf{Q}\ \mathbf{U}\ \mathbf{V}]$ was calculated pixel by pixel from the images acquired at different analyzer settings. In the Stokes vector, $\mathbf{I}$ represents the intensity of the remitted, collected light; $\mathbf{Q}$ is the difference in intensities between the horizontal ($\mathbf{I}_0$) and vertical ($\mathbf{I}_{90}$) linearly polarized components $\mathbf{U}$ is the difference in intensities between linearly polarized components traveling at +45 deg ($\mathbf{I}_{+45}$) and −45 deg ($\mathbf{I}_{-45}$) with respect to the x axis; and $\mathbf{V}$ is the difference in intensities between right ($\mathbf{I}_{\mathrm{rcp}}$) and left ($\mathbf{I}_{\mathrm{lcp}}$) circularly polarized light.

Using the Stokes components, the degree of linear polarization of the remitted light was calculated:

$$\text{degree of linear polarization} = \frac{(\mathbf{Q}^2 + \mathbf{U}^2)^{1/2}}{\mathbf{I}}.$$

A degree of linear polarization value equal to 1 corresponds to completely linear polarized light, whereas a degree of polarization value equal to 0 corresponds to light with no linear polarization characteristics. A standard color look-up table (Fire, ImageJ, National Institutes of Health) was applied to the image maps to show the different levels of polarization. The histograms of the image maps were expanded so the levels would make the best use of the color look-up table and display with sufficient contrast. The histogram expansion did not result in any loss of information regarding the polarization properties of the light remitted from the rat tail.

2.4 *Protocol for Data Collection*

Data were collected systematically for each incident polarization angle and each rat tail orientation. To construct degree of polarization image maps at a specific incident polarization angle and a specific rat tail orientation, images were acquired with the six analyzer settings. The rat tail was rotated from 0 to 360 deg in 30-deg increments. The rat tail orientation angle (ϕ) is defined as the direction of whichever end the rat tail was pointing within the range of 0 to 180 deg. For each rat tail orientation position, the incident polarization angle (IPA) was varied from 0 to 180 deg in 10-deg increments. As a result, 216 different combinations of the IPA and rat tail orientation angle were investigated. More generally though, because the rat tail was embedded in gelatin at a 15-deg angle, to completely describe the rat tail geometry, the rat tail orientation angle plus the tilt of the rat tail must be included together. Therefore, as the rat tail orientation angle was varied, the geometry of the rat tail could be described in three ways: tail laying normal to the light source (i.e., positioned such that the end of the tail nearest the source was closer to

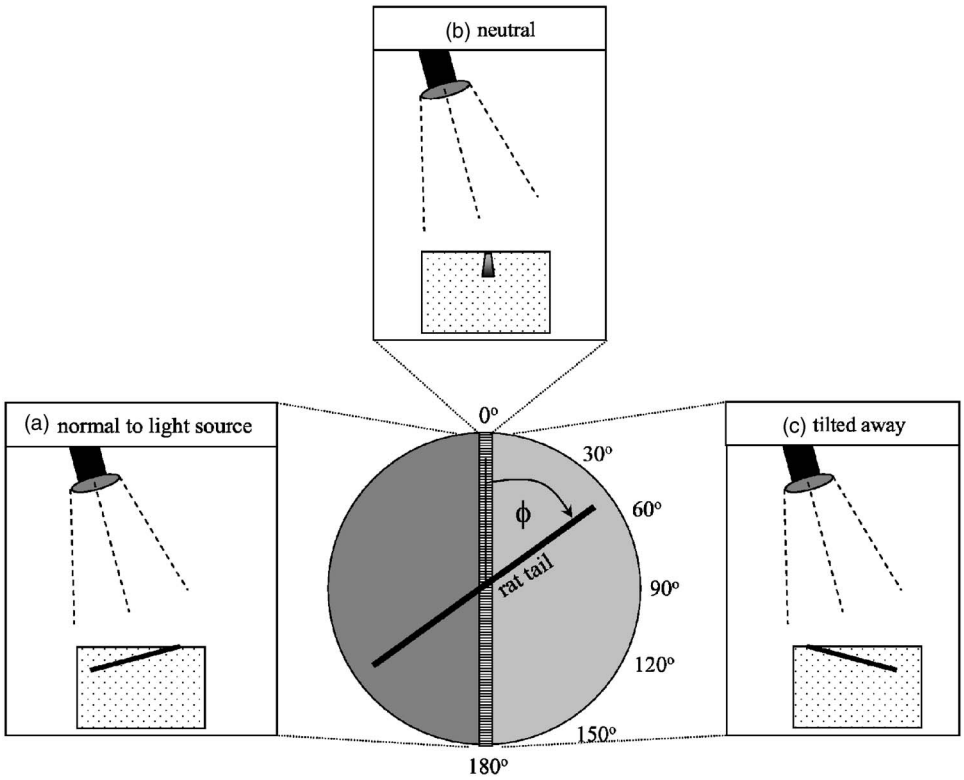

Fig. 3 Rat tail orientation angle (ϕ) and rat tail geometry defined with respect to the experimental setup. In this setup, the light source was located to the left of the rat tail axis of rotation. Rat tail geometry consisted of three general classifications: (a) rat tail tipped so that it is normal to the light source, (b) tail in a neutral position with respect to light source such that neither the more deeply embedded end nor the near-surface end was tipped away from or toward the source (ϕ=0 or 180 deg), and (c) tail tilted away from the light source such that the more deeply embedded end was further from the source.

the table top than the opposite end), tail tilted 30 deg away from the light source (i.e., positioned such that the tail end nearest the source was further from the table top than the opposite end), and the tail in a neutral position with respect to the light source (i.e., the length-wise position of the rat tail is not
preferentially tilted toward or away from the light source) (see Fig. 3).

2.5 *Rat Tail Anatomy*

To understand the polarization image maps that are presented in the results in Sec. 3, one must understand the anatomy of the rat tail.[29–32] Tendons, soft connective tissue, intervertebral disks, and caudal vertebrae are organized within the tail, as illustrated in Fig. 4. Four tendons, located around the circumference of the tail, run along the long axis of the rat tail. The tendons lie outside soft connective tissue and vertebrae structures. The vertebrae provide the rat tail with structural rigidity and periodic attachment points for the tendons. The shape of each vertebral bone resembles an hourglass, narrow near the center and wide near the ends. Each vertebra has spinous processes (not shown in Fig. 4) to which the tendons attach. Soft connective tissue covers the vertebra and fills the space between the bones and tendons. The central region of each vertebra has a narrow diameter, thus there is a relatively thick layer of soft connective tissue in this region. Conversely, the ends of each vertebra are larger in diameter; a much thinner layer of soft tissue surrounds the ends of the vertebra. Intervertebral disks are located between the vertebrae and allow the rat tail to bend its tail. The outer surface of each disk is called the annulus fibrosis and is composed of fibrous tissue

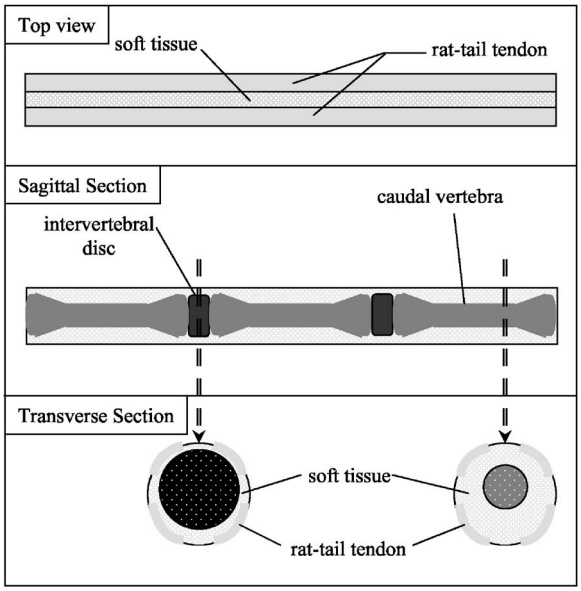

Fig. 4 Illustrations of rat tail anatomy.

and fibrocartilage. More specifically, the annulus fibrosis consists of concentric rings of fibers, where each layer of fibers pass in opposite directions. In summary, these structures form four different anatomical arrangements of tissue layers in a rat tail: 1. tendon—thick layer of soft tissue—vertebra, 2. tendon—thin layer of soft tissue—intervertebral disk, 3. soft tissue—vertebra, and 4. soft tissue—intervertebral disk. In general, at the midsection of each of the vertebra, the mean pathlength for light to reach the vertebra was relatively long because of the thick layer of tissue that exists between the tendon and the vertebra. However, at the ends of the vertebra, the mean pathlength for light to reach the vertebra or the intervertebral disk was relatively short, because only a thin layer of connective tissue exists between the tendon and the vertebra.

3 Results

The degree of linear polarization image maps of the remitted light from rat tail tissue showed several morphologies. The results are presented in the following three sections. Each section describes the observed morphologies for a particular geometry of the rat tail with respect to the light source. The images presented in each section are degree of linear polarization image maps that are representative of the type of morphologies observed.

Table 1 shows two grayscale-coded matrices describing the various morphologies observed from degree of linear polarization (DoLP) image maps in relation to the rat tail orientation angle (ϕ). Note the different morphologies observed for different incident polarization angles (IPAs). The morphologies were categorized into the following labels: band type 1, band type 2, all depolarized, tendon, mixture. These morphologies are also indicated in Fig. 5, with arrows indicating the regions along the rat tails that typify a specific morphology. Also, it is important to recognize that as the rat tail orientation angle changed, the range of IPAs at which certain morphologies could be observed shifted accordingly. Hence, in the images and in the following text, the IPA was more appropriately written as an expression in relation to the rat tail orientation angle than as a lone numerical angle.

3.1 *Tail Tilted Away from the Light Source*

Three different morphologies are observed with the rat tail placed in this geometry. Figure 5(b) shows a representative DoLP image map of the rat tail where the incident polarized light (IPA = ϕ+40 deg) had undergone strong depolarization during interaction with the rat tail tissue. The shape of the rat tail is shaded by dark pixels, and no information is revealed regarding rat tail structure besides its basic shape and outline. The dark pixels indicate that the incident polarized light had been significantly depolarized when interacting with the rat tail tissue, and that the remitted light retained very little of its initial polarization. This morphology is categorized as "all depolarized," as indicated in Table 1.

Figure 5(c) shows a representative DoLP image map where the parallel tendons running the length of the rat tail are observed to a depth of approximately 18 mm below the surface. Between the parallel tendons lay a narrow strip of soft tissue. In this image map, an IPA of ϕ+90 deg was used. This morphology was categorized as "tendon," because only the tendons along the length of the rat tail are obvious.

When light with IPAs of ϕ interacted with the rat tail tissue, one observes not only parallel tendons but also a regular banding pattern along the length of the tail [see Fig. 5(a) categorized as band type 1]. The banding pattern is observed to a depth of approximately 13 mm below the surface of the turbid gelatin, at which point there is insufficient contrast to discern the banding from the tendon.

Note that with IPA of ϕ, the DoLP at the location of the bands is significantly lower compared to the DoLP of the adjacent regions along the tendon, as displayed in Fig. 5(a). Conversely, with IPA of ϕ+90 deg [Fig. 5(c)], the DoLP measurements do not show significant changes along the length of the tendon.

Not surprisingly, the range of IPAs at which certain morphologies are observed shift according to the orientation angle of the rat tail. For example, the parallel tendons are observed when the IPA was within 90 to 140 deg for ϕ=30 deg. But when ϕ=60 deg, a shift of 30 deg, the parallel tendons are observed when the IPA was within 120 to 170 deg (i.e., centered at ϕ+80 deg) (see Table 1). Naturally, as the IPA changed there was a transition from one morphology to another; this transition is indicated by the tilde (i.e., ~) in Table 1.

3.2 *Tail Tilted Toward the Light Source*

Two distinct morphologies arose when the rat tail was tilted toward the light source. The first morphology consisted of signals remitted from the rat tail that were significantly depolarized, therefore providing information only about the general shape of the rat tail [categorized as "all depolarized," Fig. 5(e)]. This morphology looks identical to the morphology that resulted from the rat tail oriented away from the light source [Fig. 5(b)]. The range of IPAs at which this "all depolarized" morphology occurred was between, ϕ+40±5 deg. In contrast, with the rat tail tilted toward the source, the range of IPAs at which all depolarized morphology occurred was between ϕ+40±10 deg.

The second morphology consisted of signals primarily from the parallel tendons, although relatively weak depolarization signals from bands running width-wise were interspersed along the length of the rat tail [Figs. 5(d) and 5(f)]. These bands appear less prominent and wider than the ones observed previously in Fig. 5(a). The parallel tendons are observed to a depth of approximately 19 mm. So, unlike the two morphological variations observed with IPAs of ϕ and ϕ+90 deg when the tail was tilted away from the light source, in the image maps with the tail tilted toward the light source, only one type of morphology (categorized as "mixture") is present over the range of IPAs.

3.3 *Tail in Neutral Position with Respect to Light Source*

The DoLP image maps for this tail orientation consisted of two types of morphologies. The morphologies considered "all depolarized," as seen in Fig. 5(h), are similar in appearance to the morphologies previously described in Figs. 5(b) and 5(e). The rest of the morphologies, as seen in Figs. 5(g) and 5(i), categorized as "band type 2" have a banding pattern that is

Table 1 Morphologies observed in DoLP mappings at various incident polarization angles, rat tail orientation angles, and rat tail geometries. "Band type 1" indicates that there is a regularly occurring banding pattern indicating alternating regions of polarization and depolarization of remitted light along the length of the tail [see Fig. 5(a)]. "Band type 2" indicates that there is a regularly occurring banding pattern similar to that observed in "band type 1" with the exception that the depolarization of light at these banded regions was not as distinct [see Figs. 5(g) and 5(i)]. "Tendon" indicates that only the parallel tendons running the length of the rat tail are observed [see Fig. 5(c)]. "All depolarized" indicates that the light remitted from all sections of the rat tail is significantly depolarized. Besides the basic shape of the tail, no rat tail or tissue structures can be discerned [see Figs. 5(b), 5(e), and 5(h)]. "Mixture" indicates that a morphology that is a combination of the morphologies "band" and "tendon," where the parallel tendons running the length of the rat tail, are interspersed by weakly depolarized regions [see Figs. 5(d) and 5(f)]. ~ indicates an intermediate morphology. Polarizer angle tolerance = ±1 deg; polarizer angle tolerance = ±1 deg.

Incident Polarization Angle	Rat-tail Orientation Angle (ϕ)						
	Neutral position 0°	*Rat-tail tilted away from the light source* 30°	60°	90°	120°	150°	*Neutral position* 180°
0°	band - type II	~band - type I	all depolarized	tendon	all depolarized	~band - type I	band - type II
10°	band - type II	band - type I	all depolarized	tendon	tendon	all depolarized	band - type II
20°	~band - type II	band - type I	all depolarized	tendon	tendon	all depolarized	band - type II
30°	all depolarized	band - type I	~band - type I	all depolarized	tendon	all depolarized	~band - type II
40°	all depolarized	band - type I	band - type I	all depolarized	tendon	tendon	all depolarized
50°	all depolarized	~band - type I	band - type I	all depolarized	tendon	tendon	all depolarized
60°	band - type II	all depolarized	band - type I	~band - type I	all depolarized	tendon	~band - type II
70°	band - type II	all depolarized	band - type I	band - type I	all depolarized	tendon	band - type II
80°	band - type II	all depolarized	~band - type I	band - type I	all depolarized	tendon	band - type II
90°	band - type II	tendon	all depolarized	band - type I	~band - type I	tendon	band - type II
100°	band - type II	tendon	all depolarized	band - type I	band - type I	all depolarized	band - type II
110°	~band - type II	tendon	all depolarized	band - type I	band - type I	all depolarized	band - type II
120°	all depolarized	tendon	tendon	~band - type I	band - type I	all depolarized	~band - type II
130°	all depolarized	tendon	tendon	all depolarized	band - type I	~band - type I	all depolarized
140°	all depolarized	~tendon	tendon	all depolarized	~band - type I	band - type I	all depolarized
150°	~band - type II	all depolarized	tendon	all depolarized	all depolarized	band - type I	~band - type II
160°	band - type II	all depolarized	tendon	tendon	all depolarized	band - type I	band - type II
170°	band- type II	all depolarized	tendon	tendon	all depolarized	band - type I	band - type II

Incident Polarization Angle	Rat-tail Orientation Angle (ϕ)				
	Rat tail tilted toward the light source 30°	60°	90°	120°	150°
0°	mixture	mixture	mixture	mixture	mixture
10°	mixture	all depolarized	mixture	mixture	all depolarized
20°	mixture	all depolarized	mixture	mixture	all depolarized
30°	mixture	mixture	mixture	mixture	mixture
40°	mixture	mixture	all depolarized	mixture	mixture
50°	mixture	mixture	all depolarized	mixture	mixture
60°	mixture	mixture	mixture	mixture	mixture
70°	all depolarized	mixture	mixture	all depolarized	mixture
80°	all depolarized	mixture	mixture	mixture	mixture
90°	mixture	mixture	mixture	mixture	mixture
100°	mixture	all depolarized	mixture	mixture	all depolarized
110°	mixture	all depolarized	mixture	mixture	all depolarized
120°	mixture	mixture	mixture	mixture	mixture
130°	mixture	mixture	all depolarized	mixture	mixture
140°	mixture	mixture	all depolarized	mixture	mixture
150°	mixture	mixture	mixture	mixture	mixture
160°	all depolarized	mixture	mixture	all depolarized	mixture
170°	all depolarized	mixture	mixture	all depolarized	mixture

less distinct but otherwise similar to the "band type 1" morphology. The bright regions from the adjacent tendon regions are still easily visible to a depth of 12 mm.

4 Discussion

This study focused on the degree of linear polarization measurements of backscattered light collected from collagenous-type tissue, namely rat tail tissue, within a turbid medium. By varying the incident polarization angle (IPA), we found that tissue structures with polarization-sensitive characteristics remit light with different polarization properties. In addition, we found that the rat tail geometry with respect to the light source affects the polarization properties of the remitted light and the features of the tissue that can be viewed.

The interaction of the light with the rat tail tissue was uniquely dependent on the IPA. Because our setup had the incident angle of illumination tilted 15 deg with respect to the detection optics, the specular reflection was directed away from the detector. It is important to note that the detection optics selectively measured remitted photons that backscat-

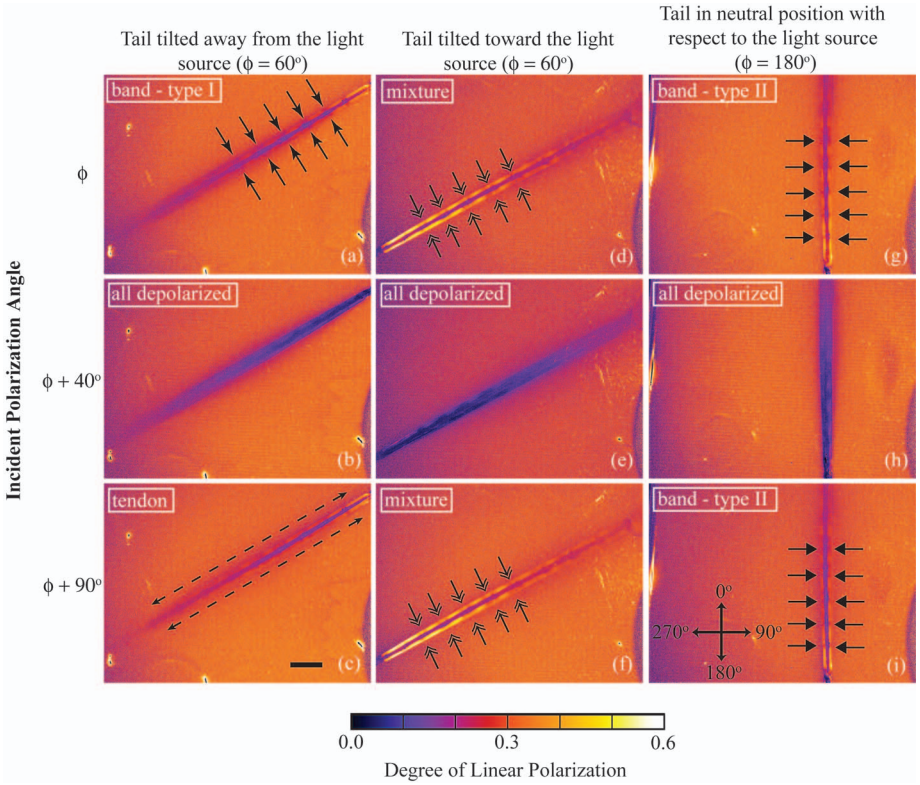

Fig. 5 Degree of linear polarization image maps at various incident linear polarization angles, rat tail orientation angles, and rat tail geometries. Refer to Table 1 for further description of images. The numerical IPAs for the images in this figure are: (a) IPA=60 deg, (b) IPA=100 deg, (c) IPA=150 deg, (d) IPA=60 deg, (e) IPA=100 deg, (f) IPA=150 deg, (g) IPA=180 deg, (h) IPA=220 or 40 deg, and (i) IPA=270 or 90 deg. The reference bar in (c) indicates a distance of 10 mm. The directional arrows in (i) indicates the angles of reference for the incident polarization angles and the rat tail orientation angles (ϕ).

tered within a range of ±1 deg with respect to the vertical axis. Thus, only a narrow cone angle of only diffusely backscattered light was detected.

Both the degree of linear polarization (DoLP) image maps and the degree of circular polarization (DoCP) image maps provide a unique perspective on the polarization properties of light from the tissue; however, for this work only the DoLP results are discussed. This study utilized linearly polarized light for illumination, and thus it was expected that DoLP image maps would contain greater signal remitted than the DoCP image maps. Degree of total polarization image maps are not shown in this work. The contribution from **Q** and **U** to the degree of total polarization was much greater than the contribution from **V**. Therefore, the degree of total polarization image maps resembled the degree of linear polarization image maps.

A bright area on the degree of polarization image maps indicates that the region of tissue remitted light with a significant state of linear polarization, while a darker area on the degree of polarization image maps indicates that the region of tissue remitted light that was not linearly polarized. Quantitatively, a bright area indicates that for two complementary analyzer angles (e.g., for **Q**, $\mathbf{I}_0$, and $\mathbf{I}_{90}$), there is a large difference in intensities; therefore, during the calculations for **Q**, **U**, or **V**, the resulting values for these elements of the Stokes vector are very high. In contrast, the dark areas show that for complementary analyzer angles, there is little difference in the intensity of light from that region, e.g., for DoLP, $\mathbf{I}_0 \approx \mathbf{I}_{90}$ and $\mathbf{I}_{45} \approx \mathbf{I}_{-45}$.

In this experiment, polarized light penetrated through the turbid gelatin and interacted with the tendon as well as the underlying tissue that included the intervertebral disks, the caudal vertebrae, and soft connective tissue. Polarized light interaction with rat tail tendon showed a dependence on the IPA. When the rat tail was rotated, not surprisingly, there was an identical shift in the morphology pattern (Table 1). Further, with the rat tail geometry in a neutral position, the occurrences of the various observed morphologies did not change for different ϕ. In fact, the occurrences of the morphologies are observed at approximately the same IPA ranges.

The reason for this dependent relationship between observed morphologies and IPA is due to linear birefringence.[27,29–35] Rat tail tendon is made up of collagen fiber bundles, where each bundle is comprised of collagen fibrils. Collagen fibers have been shown to exhibit linear birefringence.[33–35] A medium where the speed of light is a function of the electric field orientation of the traveling wave relative to the optical axes of the linearly anisotropic medium can be considered linearly birefringent. In tendon, the optical axes are orthogonal and thus, there are two different refractive indices n_x and n_y. n_x is the index of refraction in the direction perpendicular to the length of the fibrils, and n_y is the index of refraction in the direction parallel to the length of the fibrils. Experimental studies have found that linear birefringence

Table 2 Mean angle of incidence and normalized pathlength for different rat tail geometries.

	Tilted away from the light source	Tilted toward the light source	Tail in neutral position
Mean angle of incidence from normal	30 deg	0 deg	15 deg
Normalized pathlength	2.00	1.00	1.04

(Δn) is in the range of 1.0 to 3.0×10^{-3}, where $n_y > n_x$.[34,35] Although this study is concerned with collagen aligned linearly in a rat tail, the results can be extrapolated to other tissue types that contain collagen. For example, the peritoneum, a location where endometrial lesions implant in individuals with endometriosis, contains collagen fibers in a regularly organized pattern. It is expected that light remitted from the peritoneum would also exhibit dependence on the IPA just as from that of tendon, and any variation or discontinuity in the peritoneal matrix would signify a pathologic condition.

For all rat tail orientation angles, there is a range of IPAs centered around $\phi+45$ deg and $\phi+135$ deg, where the degree of polarization image maps indicate that the light was largely depolarized, [see Figs. 5(d)–5(f)]. For these IPAs, the rat tail tendon remitted light that did not have a dominant polarization, either linear or circular. So for any two complementary analyzer angles, the difference in intensities of the detected light was nearly zero. Different rat tail geometries also had no effect on the observed polarization state of remitted light at these relative IPAs. These observations can be attributed to the linear birefringence of the rat tail tendon. When IPAs of $\phi+45$ deg and $\phi+135$ deg were incident on the tendon, the orthogonal E-fields that traveled along the two different refractive indices were approximately equal. As a result, phase shifts were introduced into the linearly polarized light. These phase shifts, compounded with the multiple scattering events within the tissue, caused the polarization of the incident light to be significantly changed. At IPAs of $\phi+45$-deg and $\phi+135$-deg angles, the maximum amount of phase shift was imparted into electric field components of the light. For IPAs slightly greater or less than these angles, the amount of phase shift was less; however, significant depolarization still occurred. The IPAs could be changed, either increased or decreased, until this birefringence effect no longer caused the light to be significantly depolarized over the entire area of the tail.

When IPAs were closely centered around angles that corresponded to the optical axes of the tendon, either at ϕ (parallel to the length of the collagen fibers) or at $\phi+90$ deg (perpendicular to the length of the collagen fibers), the incident polarization of the light was not significantly depolarized. With these IPAs, the electric field interacted with the tendon at a relatively constant refractive index and allowed the polarized light propagation to maintain a large degree of its linearity. To obtain a signal from tissue located underneath the tendon, light must be transmitted or forwardscattered through the tendon, backscatter off the underlying tissue, and pass back out of the tendon. For rat tail tissue, the intervertebral disks and the caudal vertebrae possess highly scattering materials: hydroxyapitite crystals and fibrous collagen. Comparatively, though, the soft connective tissue is not as highly scattering in the backward direction.[36]

Examining the region of the rat tail between the two tendons corroborates the idea that the soft tissue scrambled the polarization of the incident light. In this central region, there was a layer of soft tissue that lay above either vertebrae or intervertebral disks. As seen in all image maps, the central region remains dark for all IPAs.

In the degree of linear polarization image maps, when the tail was tilted 30 deg away from the light source, two interesting morphologies appear when the IPA was ϕ or $\phi+90$ deg. When IPA was ϕ, dark bands are seen along the length of the tail. But when the IPA was $\phi+90$ deg, the dark bands are not present and only the parallel tendons are the primary structures observed. These observations can be attributed to linear dichroism inherent in tendon.[37,38] Linear dichroism is the difference in the absorbance of linearly polarized light when the axis of the material is parallel of perpendicular to the plane of polarized light. When the IPA was parallel to the axis of the rat tail, the absorption of the tendon was minimal, but when the IPA was perpendicular to the axis of the rat tail, absorption was greater. Therefore, with an IPA of ϕ, the polarized light had a greater chance of penetrating deeper into the rat tail and to interact with the intervertebral disk. With an IPA of $\phi+90$ deg, the polarized light was sufficiently absorbed by the dichroic tendon, and so significantly less light reached the intervertebral disk; hence, the banding pattern was not present in these image maps. However, one should notice that a banding pattern is observed in the DoLP image maps with IPA of either ϕ or $\phi+90$ deg when the tail was in a neutral position [Figs. 5(g) and 5(i)]. In addition, a weaker banding morphology is observed with IPA of either ϕ or $\phi+90$ deg when the tail was tilted toward the light source [Figs. 5(d) and 5(f)]. These results may be initially counterintuitive, but further analysis indicates that the explanation to these observations lies in the angle of incidence of the polarized light with the tendon. For example, when the tail was tilted away from the light source, the most direct path for light to propagate through tendon was longest (see Table 2). Because of the longer pathlength, the light encountered greater absorbance when IPAs of $\phi+90$ deg were used. However, when the tail was in a neutral position, polarized light with IPAs of $\phi+90$ deg encountered about two times less absorbance. Because of this, light could propagate without being attenuated significantly by the tendon, and then interact with

the intervertebral disk. In other words, the effects due to dichroism were minimal for this geometry. The same reasoning can be applied to explain the observed morphologies when the tail was tilted toward the light source. In this case, however, there were stronger polarization signals from the tendons, including the regions that were directly above the intervertebral disks. The banding morphology in the image maps were slightly less distinct because of this, but nevertheless noticeable. Further goniometric studies of isolated tendon could be performed in the future to fully characterize this dichroic effect and the absorptivity as a function of angle of incidence. The results indicate that to obtain the information about subsurface tissue structures, the angle of incidence needs to be varied. A Stokes polarimetry imaging device developed for clinical use should vary the angle of incidence, so that acquired images yield a more complete characterization of the region of interest.

In general, light that interacted with intervertebral disk became depolarized. The annulus fibrosis encasing the soft gelatinous center of the disk significantly depolarized the light. These findings are important, since pathological tissue may also contain fibrosis or scarring in its matrix. Endometrial lesions exhibit these fibrotic characteristics and one would expect that locations of these lesions would remit depolarized light compared to the normal surrounding tissue.

5 Conclusion

These results indicate that by using Stokes polarimetry imaging, the IPAs, tissue orientation angle, and geometry of the tissue with respect to the polarized light source contribute to the characterization of tissue in DoLP image maps. One must recognize that the polarization of remitted light is not only influenced by the superficial tissue layers, but also by the underlying tissue layers. Hence, this imaging technique may provide utility in subsurface tissue imaging. Future work could involve clinical applications where this imaging technique is applied to regions of tissue, on the order of several square centimeters, or to the exterior of organs to distinguish pathological changes or abnormalities. As many previous polarization studies have concentrated on just the orthogonal polarization components, we believe that this study shows the benefit of imaging with multiple incident polarization angles. Further, whereas other techniques provide high resolution information only to a millimeter or so below the tissue surface [e.g., Optical Coherence Tomography (OCT)], the technique described here yields information to deeper depths and at higher image capture rates over a larger surface area. In this basic study, the entire rat tail, including the tendons, was oriented in a linear fashion. However, other tissue types, either normal or atypical, in other settings may present a tissue structure that is not oriented exclusively in a linear fashion. For example, the general orientation of collagen fibers may be aligned at many different angles. Therefore, the interrogation of the tissue using multiple incident polarization angles, intermediate to orthogonal states, may show greater functionality in gleaning information on polarization-sensitive structures than if imaged with a single polarization.

Acknowledgments

This research was supported in part by NIH grant R01-HD044015. The authors would like to thank Magdy Milad for useful discussions regarding endometriosis pathology and detection.

References

1. S. P. Morgan, M. P. Khong, and M. G. Somekh, "Effects of polarization state and scatterer concentration on optical imaging through scattering media," *Appl. Opt.* **36**(7), 1560–1565 (1997).
2. J. M. Schmitt, A. H. Gandjbakhche, and R. F. Bonner, "Use of polarized light to discriminate short-path photons in a multiply scattering medium," *Appl. Opt.* **31**(30), 6535–6546 (1992).
3. F. C. MacKintosh, J. X. Zhu, D. J. Pine, and D. A. Weitz, "Polarization memory of multiply scattered light," *Phys. Rev. B* **40**(13), 9342–9345 (1989).
4. R. C. N. Studinski and I. A. Vitkin, "Methodology for examining polarized light interactions with tissues and tissuelike media in the exact backscattering direction," *J. Biomed. Opt.* **5**(3), 330–337 (2000).
5. I. A. Vitkin and R. C. N. Studinski, "Polarization preservation in diffusive scattering from in vivo turbid biological media: effects of tissue optical absorption in the exact backscattering direction," *Opt. Commun.* **190**, 37–43 (2001).
6. K. C. Hadley and I. A. Vitkin, "Optical rotation and linear and circular depolarization rates in diffusively scattered light from chiral, racemic, and achiral turbid media," *J. Biomed. Opt.* **7**(3), 291–299 (2002).
7. I. A. Vitkin and E. Hoskinson, "Polarization studies in multiply scattering chiral media," *Opt. Eng.* **39**(2), 353–362 (2000).
8. A. H. Hielscher, J. R. Mourant, and I. J. Bigio, "Influence of particle size and concentration on the diffuse backscattering of polarized light from tissue phantoms and biological cell suspensions," *Appl. Opt.* **36**(1), 125–135 (1997).
9. S. P. Morgan and M. E. Ridgway, "Polarization properties of light backscattered from a two layer scattering medium," *Opt. Express* **7**(12), 395–402 (2000).
10. R. R. Anderson, "Polarized light examination and photography of skin," *Arch. Dermatol.* **127**, 1000–1005 (1991).
11. S. G. Demos, H. B. Radousky, and R. R. Alfano, "Deep subsurface imaging in tissues using spectral and polarization filtering," *Opt. Express* **7**(1), 23–28 (2000).
12. S. L. Jacques, J. R. Roman, and K. Lee, "Imaging superficial tissues with polarized light," *Lasers Surg. Med.* **26**, 119–129 (2000).
13. S. L. Jacques, J. R. Roman, and K. Lee, "Imaging skin pathology with polarized light," *J. Biomed. Opt.* **7**(3), 329–340 (2002).
14. J. C. Ramella-Roman, K. Lee, S. A. Prahl, and S. L. Jacques, "Design, testing, and clinical studies of a handheld polarized light camera," *J. Biomed. Opt.* **9**(6), 1305–1310 (2004).
15. R. A. Chipman, "Polarimetry," Chap. 22 in *Handbook of Optics*, 2nd ed., M. Bass, Ed., Vol. **2**, pp. 22.1–22.37, McGraw-Hill, New York (1994).
16. D. A. Kliger, J. W. Lewis, and C. E. Randall, *Polarized Light in Optics and Spectroscopy*, Academic Press Inc., San Diego, CA (1990).
17. W. S. Bickel and W. M. Bailey, "Stokes vectors, Mueller matrices, and polarized scattered light," *Am. J. Phys.* **53**(5), 468–478 (1985).
18. E. Collett, *Polarized Light in Fiber Optics*, The Pola Wave Group, Lincroft, NJ (2003).
19. G. D. Lewis, D. L. Jordan, and P. J. Roberts, "Backscattering target detection in a turbid medium by polarization discrimination," *Appl. Opt.* **38**(18), 3937–3944 (1999).
20. A. H. Hielscher, A. A. Eick, J. R. Mourant, D. Shen, J. P. Freyer, and I. J. Bigio, "Diffuse backscattering Mueller matrices of highly scattering media," *Opt. Express* **1**(13), 441–453 (1997).
21. S. B. Bartel and A. H. Hielscher, "Monte Carlo simulations of the diffuse backscattering Mueller matrix for highly scattering media," *Appl. Opt.* **39**(10), 1580–1588 (2000).
22. J. S. Baba, J. R. Chung, A. H. DeLaughter, B. D. Cameron, and G. L. Cote, "Development and calibration of an automated Mueller matrix polarization imaging system," *J. Biomed. Opt.* **7**(3), 341–349 (2002).
23. M. H. Smith, P. Burke, A. Lompado, E. Tanner, and L. W. Hillman, "Mueller matrix imaging polarimetry in dermatology," *Proc. SPIE*

3911, 210–216 (2000).
24. J. Li, G. Yao, and L. V. Wang, "Degree of polarization in laser speckles from turbid media: Implication in tissue optics," *J. Biomed. Opt.* **7**(3), 307–312 (2002).
25. C. W. Sun, C. C. Yang, and Y. W. Kiang, "Optical imaging based on time-resolved Stokes vectors in filamentous tissues," *Appl. Opt.* **42**(4), 750–754 (2003).
26. V. Sanakaran, K. Schnenberger, J. T. Walsh, Jr., and D. J. Maitland, "Polarization discrimination of coherently propagating light in turbid media," *Appl. Opt.* **38**(19), 4252–4261 (1999).
27. V. Sankaran, J. T. Walsh, Jr., and D. J. Maitland, "Comparative study of polarized light propagation in biological tissues," *J. Biomed. Opt.* **7**(3), 300–306 (2002).
28. T. J. Farrell and M. S. Patterson, "A diffusion theory model of spatially resolved, steady-state diffuse reflectance for the noninvasive determination of tissue optical properties in vivo," *Med. Phys.* **19**(4), 879–888 (1992).
29. U. E. Pazzaglia, L. Andrini, and A. Di Nucci, "The effects of mechanical forces on bones and joints," *J. Bone Joint Surg. Br.* **79B**(6), 1024–1030 (1997).
30. G. Ellender, S. A. Feik, and B. J. Carach, "Periosteal structure and development in a rat caudal vertebra," *J. Anat.* **158**, 173–187 (1988).
31. R. W. Thorington, Jr., "The biology of rodent tails: a study of form and function," PhD Thesis, Dept. of Biology, Harvard Univ., Cambridge, MA (1966).
32. G. J. Krinke, *The Laboratory Rat*, Academic Press, New York (2000).
33. D. J. Maitland and J. T. Walsh, Jr., "Quantitative measurements of linear birefringence during heating of native collagen," *Lasers Surg. Med.* **20**, 310–318 (1997).
34. G. J. van Blokland and S. C. Verhelst, "Corneal polarization in the living human eye explained with a biaxial model," *J. Opt. Soc. Am. A* **4**, 82–90 (1987).
35. A. Stanworth and E. J. Naylor, "Polarized light studies in cornea. I. The isolated cornea," *J. Exp. Biol.* **30**, 160–163 (1953).
36. W. F. Cheong, S. A. Prahl, and A. J. Welch, "A review of the optical properties of biological tissues," *IEEE J. Quantum Electron.* **26**, 2166–2185 (1990).
37. V. L. C. Feitosa, B. C. Vidal, and E. R. Pimental, "Optical anisotropy of a pig tendon under compression," *J. Anat.* **200**, 105–111 (2002).
38. M. L. S. Mello, B. C. Vidal, A. C. de Carvalho, and A. C. Caseiro-Filho, "Change with age of anisotropic properties of collagen bundles," *Gerontology* **25**(2), 2–8 (1979).